Nationaal Lucht- en Ruimtevaartlaboratorium
National Aerospace Laboratory NLR

NLR TP 97304

Determination of transonic unsteady aerodynamic loads to predict the aeroelastic stability of fighter aircraft.

J.J. Meijer

DOCUMENT CONTROL SHEET

	ORIGINATOR'S REF.		SECURITY CLASS.
	TP 97304 U		Unclassified

ORIGINATOR
National Aerospace Laboratory NLR, Amsterdam, The Netherlands

TITLE
Determination of transonic unsteady aerodynamic loads to predict the aeroelastic stability of fighter aircraft.

PRESENTED AT
the International Forum on Aeroelasticity and Structural Dynamics, Rome, Italy, June 17-20, 1997

AUTHORS	DATE	pp	ref
J.J. Meijer	970601	14	15

DESCRIPTORS

Aeroelasticity	Nonlinearities	Transonic flutter
Dynamic models	Parameter identification	Vibration damping
External stores	Prediction analysis techniques	Wing oscillations
Fighter aircraft	Pressure distribution	Wing flaps
Hysteresis	Time lag	

ABSTRACT
A model for determining aerodynamic loads from steady and unsteady data bases is presented that is suitable for predicting Limit Cycle Oscillations (LCO) of fighter aircraft at transonic speeds. Validations of the model will be presented, in particular the influence of Mach number variations, different control flap settings and oscillation frequency and amplitude are demonstrated. A few examples of the aerodynamic model embedded in the LCO prediction method are presented to show the LCO characteristics of a fighter type aircraft. Finally, enhancement of the use of the model will be discussed by extension of the data bases with data obtained from CFD methods and/or new wind tunnel experiments.
Key words: Aeroelasticity, Strucutral Dynamics, Transonic Limit Cycle Oscillations, Transonic Unsteady Airloads

Determination of Transonic Unsteady Aerodynamic Loads to Predict the Aeroelastic Stability of Fighter Aircraft

Jos J. Meijer
NLR, Anthony Fokkerweg 2, 1059CM Amsterdam, NL
email: meijer@nlr.nl

Abstract. A model for determining aerodynamic loads from steady and unsteady data bases is presented that is suitable for predicting Limit Cycle Oscillations (LCO) of fighter aircraft at transonic speeds. Validations of the model will be presented, in particular the influence of Mach number variations, different control flap settings and oscillation frequency and amplitude are demonstrated. A few examples of the aerodynamic model embedded in the LCO prediction method are presented to show the LCO characteristics of a fighter type aircraft. Finally, enhancement of the use of the model will be discussed by extension of the data bases with data obtained from CFD methods and/or new wind tunnel experiments.

Key words: Aeroelasticity, Structural Dynamics, Transonic Limit Cycle Oscillations, Transonic Unsteady Airloads

1. Introduction

New store configurations for fighter aircraft operating in the transonic flight regime require nonlinear aeroelastic analysis to determine the possibility of Limit Cycle Oscillations (LCO). An essential aspect of this phenomenon is the nonlinear nature of the unsteady airloads and their dependence on the mean steady flow conditions. Therefore, modeling of the nonlinear aerodynamic forces is the important key to predict aircraft LCO characteristics.

One approach to determine the nonlinear aerodynamics is to apply computational fluid dynamic (CFD) techniques in the time domain where structural deflection response is accounted for simultaneously. The time varying pressure distributions are used in the closed loop structural dynamics model to determine the nonlinear structural response. Although this approach is being used to a certain extent, its applicability is limited because of the immature status of the prediction of three-dimensional unsteady separated flow and of the large computer resources required.

Another approach [1] for predicting the nonlinear aerodynamics of LCO is to develop a mathematical model that uses steady wind tunnel pressure data in combination with a description of unsteady effects. The concept is based on the idea that configuration specific effects are contained in the steady pressure data base. These effects include such items as free stream Mach number, incidence, flap settings and wing stores. Furthermore, the concept assumes that the unsteady effects are generic and can be described by an universal algorithm.

A third approach [2, 3] which makes use of measured steady and unsteady pressure data under conditions of LCO is another possibility for determining these nonlinear aerodynamic forces. The approach is based on an aerodynamic state-space modeling developed by NLR for transforming unsteady nonlinear aerodynamic loads into a form appropriate for use in time simulation methods. This method is similar to the nonlinear "ONERA" aerodynamic model initially developed by Tran & Petot [4].

The application and validation of the latter aerodynamic state-space model will be presented in this paper. First some background will be presented by analysis of steady wind tunnel data obtained for a fighter type aircraft to understand the development of LCO at transonic speeds. Different flow field types are discussed, followed by a presentation of unsteady pressure data. Next, the concept of the aerodynamic state-space model in its most recent form and its evolvement is presented, accompanied by some typical unsteady results obtained with the model to demonstrate its applicability. Finally, the influence of free stream Mach number, flap settings and oscillation frequency and amplitude will be shown followed by improvements of the model and by conclusions.

2. Nonlinear Aerodynamics for LCO

In order to identify the important nonlinearities in the aerodynamic forces that could drive LCO, steady pressure data of a full-span wind tunnel model of a typical fighter aircraft were analyzed at NLR which were made available by the aircraft manufacturer [5]. The objective of that test, the acquired pressure data, test conditions and configuration matrix were summarized in reference [2]. The wing planform of the wind tunnel model provided with pressure orifices is shown in figure 1. Also shown is the panel distribution used in the

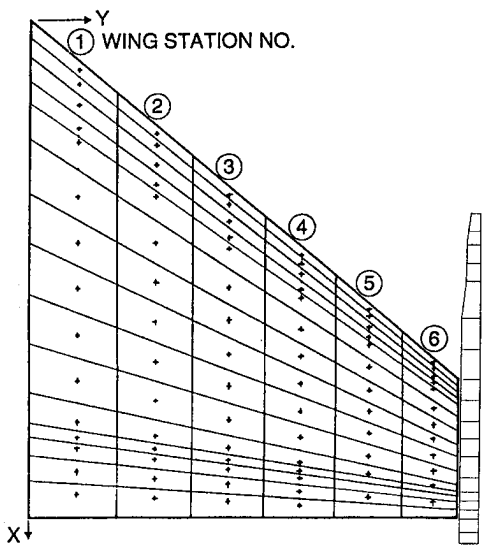

Fig. 1 Location of pressure orifices and corresponding panels on the model wing planform.

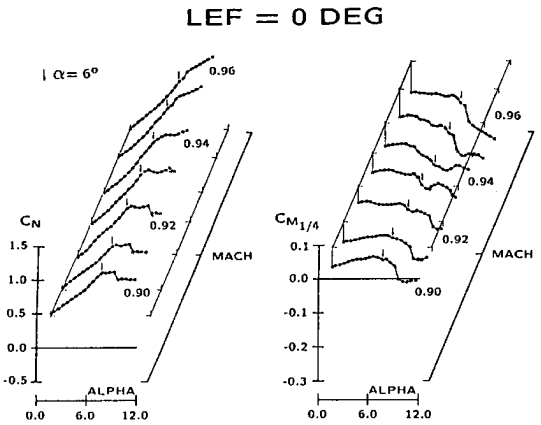

Fig. 2 Steady lift and moment coefficients at station 6 as function of Mach number and angle-of-attack

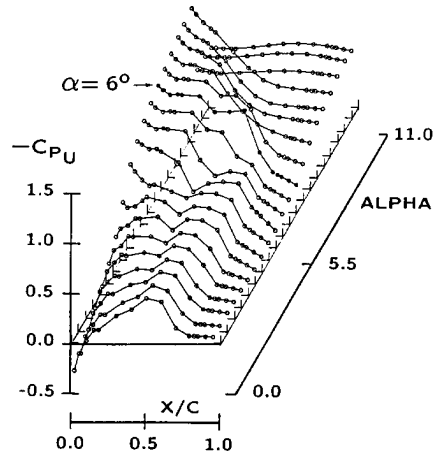

Fig. 3 Steady pressure distributions at station 6 as function of angle-of-attack ($\delta_{le} = 0$ deg, $\delta_{te} = 0$ deg), upper wing surface, M = 0.92.

chordwise and spanwise integration to obtain sectional and/or generalized aerodynamic forces.

Results of the NLR analysis are presented for one type of tip launcher and one leading-edge flap setting. In figure 2 the steady normal force and moment section coefficients are shown for station 6 (most outboard) as function of angle-of-attack (0 to 10 deg) and Mach number (0.90 to 0.96) and leading-edge flap setting of 0 deg. The lift and moment coefficients show rapid changes in short intervals of the angles-of-attack (centered on about 5 to 7 deg) in the greater part of the Mach number interval. These rapid changes are typical to drive LCO. The coefficients for the more inboard stations show a gradual transition to a more regular behavior.

To analyze the kind of pressure distributions which lead to the rapid changes in the section aerodynamic coefficients, the pressure distributions on the upper wing surface in station 6 at Mach number 0.92 are presented in figure 3. A strong upstream shift of the shock starts at about 4 to 7 deg coupled with a rapidly developing flow separation at the trailing-edge. This occurs after a merging of the weaker nose and aft shocks into a much stronger single shock that induces the extensive separation. The shock motion also reverses at this point which coincides with breaks in the sectional lift and pitching moment coefficients. The pressure distributions on the lower side show only very gradual developments.
For the other type of tip launcher and leading-edge flap settings the same kind of trends were observed.

3. Flow Field Type Identification

In order to be able to account for the effects of different flow fields on unsteady airloads, in terms of local time lags (section 4), these flow fields must first be identified [1]. This identification includes both the type and extent of each flow field. A means for accomplishing this task was developed for the pressure data base given in [5] by carefully examining pressure variations with both incidence and location and correlating these variations with available flow visualization information as well as prior knowledge of the wing flow field characteristics. The goal of the development was to obtain a method that could be applied to any set of pressure distributions to determine flow field maps with no user interaction.

The flow fields were grouped into two categories,

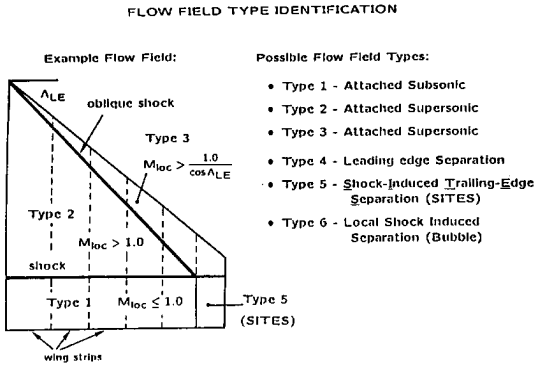

Fig. 4 Flow field type identification:
a) Example flow field for given (M,α) (left),
b) Possible flow field types (right).

attached and separated flows (Fig. 4). Three types of attached flow were defined and three types of separated flow were also defined. In figures 5a-5c the three different types of separated flows are presented. For the same wing geometry data are shown obtained from two different wind tunnel test programs, steady pressure data of the full-span test [5] and mean pressure data of the semi-span test [6]. Figure 5a shows leading-edge separation (type 4) at WS6, figure 5b separation bubble near the forward shock (type 6) at WS3 and figure 5c shock-induced trailing-edge-separation (type 5) at WS4. Further details of the flow identification are summarized in reference [1]. These flow field characteristics are important and probably, flow transitions are even more important in developing unsteady nonlinear aerodynamics.

4. Unsteady Nonlinear Aerodynamic Models

The use of unsteady aerodynamic data obtained from harmonically oscillating wind tunnel models is a practical means for solving aeroelastic problems where the aerodynamic characteristics are highly nonlinear.

Two methods are being developed for calculating unsteady nonlinear aerodynamic forces due to structural response, which make use of measured steady data for the configurations of interest. One model presents an extension of the simple aerodynamic time lag concept (LMTAS method) [1], whereas the other model comprises a state-space modeling (NLR method) [2, 3] of the unsteady aerodynamic forces. The parameters used in both methods were derived from unsteady pressure data obtained from unsteady wind tunnel test on oscil-

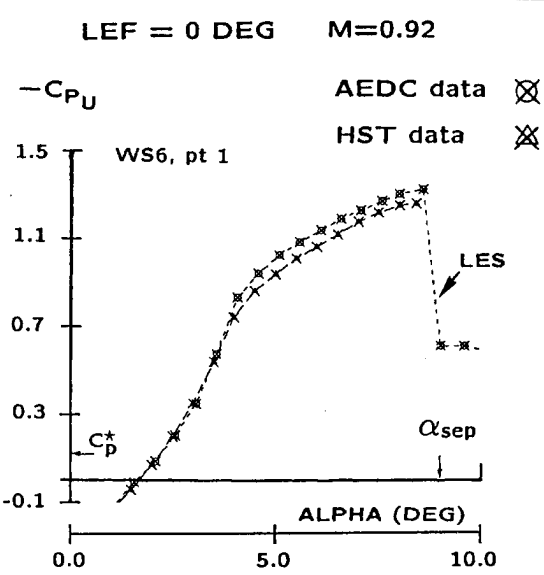

a) Leading-Edge Separation (LES)

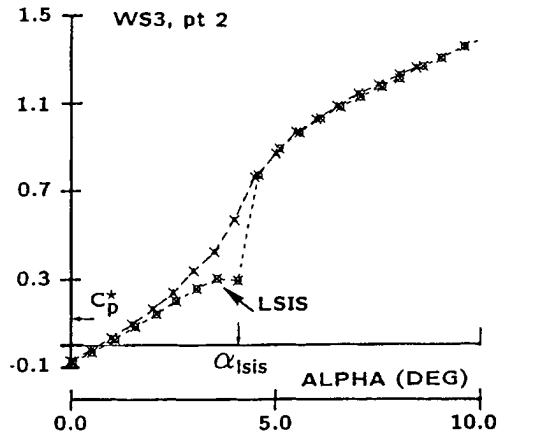

b) Local Shock Induced Separation (LSIS)

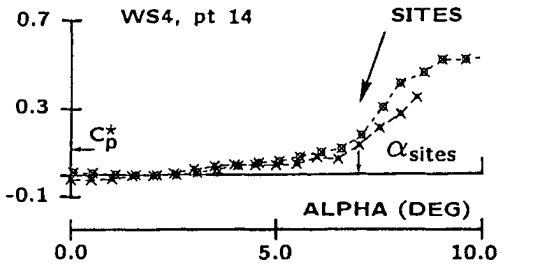

c) Shock-Induced Trailing-Edge Separation (SITES)

Fig. 5 Steady pressure data as function of angle-of-attack for determining flow field type identification.

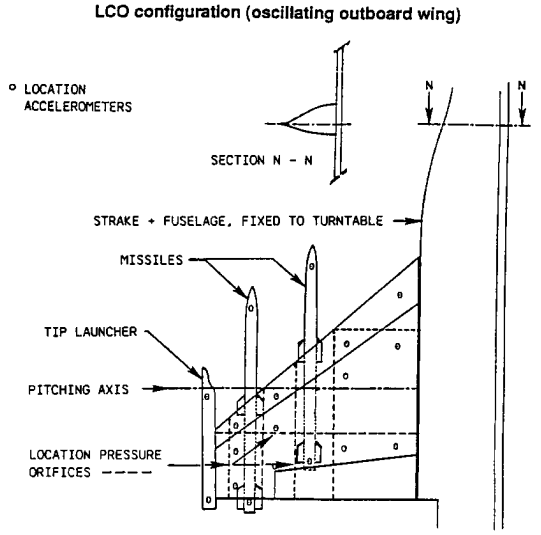

Fig. 6 Wind tunnel model of fighter type wing for LCO investigation.

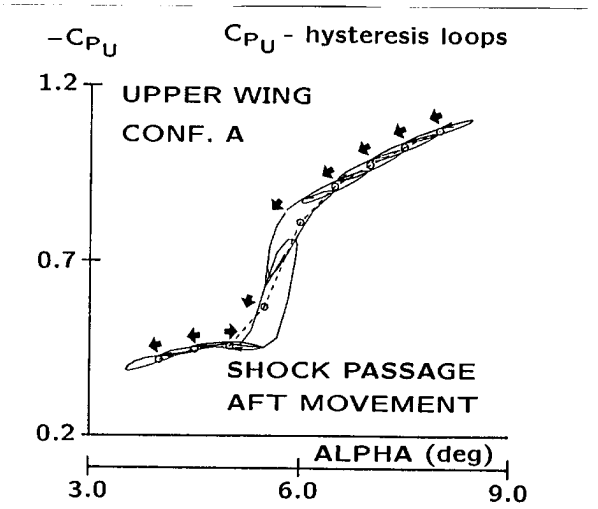

a) shock passage aft movement (WS3, pt 4)

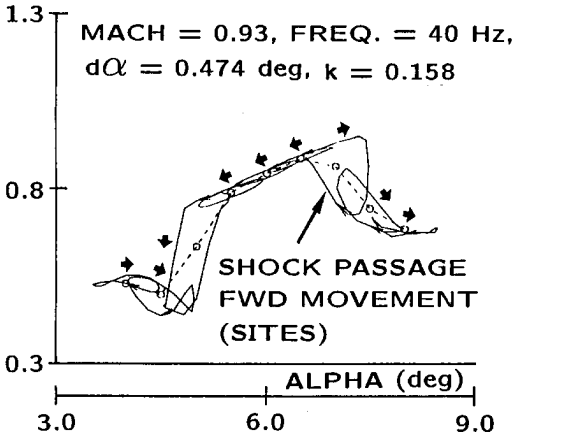

b) shock passage fwd movement (WS6, pt 7)

Fig. 7 Pressure coefficients, upper wing surface, (M=0.93), measured hysteresis loops.

lating fighter type wings [6]. The objective of that test was to obtain unsteady pressure data for the same test conditions as mentioned in section 2 for the steady pressure measurements [5]. The wing planform of the wind tunnel model (Fig. 6) and location of pressure orifices were essentially the same as shown in figure 1.

Specific requirements of the unsteady wind tunnel test were to provide: (1) steady data for reference conditions unique to the LCO wind tunnel model geometry and test setup; (2) unsteady data for harmonic pitching motion with sufficient incidence and Mach number resolution; and (3) time history recordings of unsteady data.

Correlations of the pressure data from the two tests showed very good agreement (Figs. 5a-5c) in spite of some differences in the model and test setup. It was possible to reproduce the incidence and Mach sensitive characteristics in sufficient detail to conclude that a good match between the two wind tunnel tests was achieved.

As an example for defining flow field effects on local time lag characteristics (section 3) time history plots are shown in figure 7, including a description of important flow characteristics.

When a shock develops and moves aft with increasing incidence, the characteristics shown in figure 7a between α=5 deg and 6.5 deg are obtained. The strangely shaped hysteresis loops below α=5 deg are typical of a local shock-induced separation bubble but are not significant in producing aerodynamic forces that are important to LCO. The large loops near shock passage are important and are much larger than those produced by attached supersonic flow above α=6.5 deg (supersonic normal to the leading-edge). However, both the shock and supersonic loops are counterclockwise. The outer boundary formed by the shock loops appear to form a shape that would be produced if the steady shock C_p distribution was shifted either +0.25 deg (increasing incidence or time) or -0.25 deg (decreasing incidence or time).

An even more complicated picture arises when the transition to (or from) shock-induced trailing-edge-separation (SITES) is encountered during the oscillation cycle. This characteristic is shown in figure 7b for the loop centered at α=7 deg. The hysteresis loops at α=4.5 deg and 5.0 deg are characteristic of the aft shock movement noted in figure 7b. Those at α=5.5 deg to 6.5 deg of the same figures are typical of flows supersonic normal to the

leading-edge. All of these loops are counterclockwise. The loops at α=7.0 deg are typical of SITES transition and is now clockwise because the shock is moving forward. The shape of the SITES loops is also much more circular than that for shock aft passage and is indicative of much larger time lags for flow transition.

According to the time history analyses the shape of pressure hysteresis loops varies as follows: (1) attached subsonic or supersonic flows - elliptic; (2) shock passage - varied; (3) transition to separation - varied; (4) fully separated flows - generally elliptic.

On the basis of the flow field identifications and the observed unsteady trends a state-space modeling of the unsteady pressure data was chosen at NLR and an aerodynamic time lag modeling at LMTAS.

The NLR method will be described to some extent in the following sections. Details of the LMTAS method are further discussed in reference [1].

5. Aerodynamic State-Space Model

The basic model was developed by the *Office National d'Etudes et de Recherches Aerospatiales* (ONERA) for loads at rotor blade sections operating in or near stall conditions (Refs. [4],[7]-[9]). This concept has been extended by NLR to individual pressures for a three-dimensional wing to predict LCO characteristics of fighter aircraft [2, 3].

The NLR unsteady pressure model follows along the logic discussed in [2, 3] for the ONERA model for unsteady forces. The objectives of both approaches are the same where it is desired to predict nonlinear unsteady aerodynamic forces or pressures for arbitrary wing motions.

The basic principles in figure 8 and the equations are essentially the same as those for the ONERA model, but now applied to the individual pressures

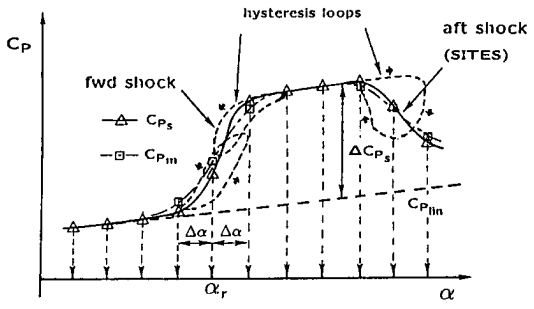

Fig. 8 "NLR" state-space pressure model concept.

over the wing area.

$$C_p\langle\tau\rangle = C_{p_1}\langle\tau\rangle + C_{p_2}\langle\tau\rangle, \tag{1}$$

$$C_{p_1}\langle\tau\rangle = C_{p_\gamma}\langle\tau\rangle + s_z \overset{*}{\alpha} + k_{vz} \overset{**}{\theta}, \tag{2}$$

$$\overset{*}{C}_{p_\gamma} + \lambda_z C_{p_\gamma} = \lambda_z \left(C_{p_{lin}}\langle\alpha\rangle + \sigma_z \overset{*}{\theta} \right) + \alpha_z \left(\frac{\partial C_{p_{lin}}}{\partial \alpha} \overset{*}{\alpha} + \sigma_z \overset{**}{\theta} \right), \tag{3}$$

$$\overset{**}{C}_{p_2} + a_z \overset{*}{C}_{p_2} + r_z C_{p_2} = r_z \left[\Delta C_p\langle\alpha\rangle + e_z \frac{\partial \Delta C_p\langle\alpha\rangle}{\partial \alpha} \overset{*}{\alpha} \right], \tag{4}$$

and

$$\Delta C_p\langle\alpha\rangle = C_{p_s}\langle\alpha\rangle - C_{p_{lin}}\langle\alpha\rangle, \tag{5}$$

where $\alpha = \theta + \overset{*}{h}/b$, $\overset{*}{(\,)} \equiv \partial(\,)/\partial\tau$ and $\tau = Ut/b$. The parameters λ_z, a_z, r_z and α_z, σ_z and s_z, k_{vz} and e_z must be determined empirically by parameter identification techniques. Additional conditions for the parameters are: $\lambda_z > 0,\ 0 < \alpha_z < 1,\ a_z > 0,\ a_z > 0,\ r_z > 0,\ e_z < 0$ and $4r_z > a_z^2$. These conditions are needed to avoid instabilities and hence facilitate the fitting procedure. The conditions for λ_z, α_z, a_z and r_z lead to constraints for α_z and e_z, i.e. to intervals in which their values should lie.

The nonlinear variation of $C_p(\tau)$ is the sum of two parts $C_{p_1}(\tau)$ and $C_{p_2}(\tau)$, where the former is primarily governed by the slope of $C_{p_{lin}}$ and the latter by ΔC_{p_s}, the difference of C_{p_s} and $C_{p_{lin}}$. In the same way as for the ONERA model the position of $C_{p_{lin}}$ was determined originally by the linear variation of C_{p_s} with α for conditions of attached flow (small incidences) where no changes occur in flow fields such as shock passages and Shock-Induced and Trailing-Edge Separation as illustrated in figure 8. However, taking into account correctly the local nonlinear features of flow fields such as shock passages, etc. (Fig. 8) at higher incidences, the meaning of $C_{p_{lin}}$, ΔC_{p_s} and their derivatives has been redefined in the NLR pressure model. This modified approach consists of locally developed $C_{p_{lin}}$ and ΔC_{p_s} with α. So, the main difference with the ONERA model is that the complete set of equations is applied at each event, i.e. no distinction is made between linear and nonlinear portions of the C_{p_s} curves. This implies that all eight unknown parameters have to be determined a priori for each reference angle-of-attack α_r and each pressure location at a given Mach number.

In [2, 3] an attempt was made to provide a physical background to the parameters in the ONERA model. This interpretation can be maintained largely in

the NLR model. Thus, it might be supposed that C_{p_1}, equations (2,3), is defined mainly by the linear variation of a steady local $C_{p_{lin}}$ and five parameters, λ_z, and α_z, σ_z and s_z, k_{vz}. These quantities account for the time delay effects as well as flow inertia effects. In the same way C_{p_2}, equation (4), is defined by the steady local nonlinear function, ΔC_{p_s}, and three parameters, a_z, r_z and e_z. These quantities account for such effects as flow separation and reattachment, time delay of flow transitions and shock-wave passage.

The solution procedure for evaluating the eight unknown parameters in the NLR pressure model at each reference angle-of-attack α_r and at each pressure location makes use of a parameter identification technique, in a similar way as was outlined in [2]. This technique implies that use is made of results of the model test in the wind tunnel during which pressures were measured due to oscillatory motion at small amplitude about some mean angle-of-attack α_r. The technique has been described in [2, 3].

Oscillatory data for about 0.5 deg amplitude, 40 Hz frequency, Mach number 0.93 and a reduced frequency of 0.158 from the unsteady wind tunnel test [6] were used to develop the parameter data base for validation purposes (next section).

The whole procedure for determining the parameters has to be repeated for each Mach number and each measured test configuration.

In the NLR unsteady aerodynamic model, time varying nonlinear C_p distributions are reconstructed for arbitrary wing motions using the above obtained parameters. The technique for reconstructing these time histories is based on a finite difference formulation of the four equations where backward differences are employed for predicting pressures at the next time step. This finite difference procedure has been implemented in the aerodynamic loads module of the LCO prediction method.

6. Application of the NLR Model

The NLR model was used to recompute the unsteady pressure distributions from which the model parameters were obtained. This gave a direct evaluation of how well the method could reproduce the data which it was attempting to fit. A few results are shown in the figures 9a to 9c, including flow characteristics to correlate with the type of hysteresis loops.

The simplest case to begin with is attached flow fields where no transitions occur. This is illustrated in figure 9a for a forward pressure location at wing station 3 on the upper surface of the wing. With a free stream Mach of 0.93, the flow at this point 1 is continuously accelerated supersonically for all angles shown from 4 deg to 8 deg. Thus, the flow field type illustrated is attached supersonic flow where the local Mach number is always supersonic normal to the wing leading-edge. The mean (static) chordwise pressure distributions also shown in figure 9a for the incidence sweep indicate that the pressure point 1 at wing station 3 (denoted by "$\otimes$") is indeed forward of the nose shock.

The format for the unsteady pressure data portrays the hysteresis loops at various mean incidences, about which the model is oscillating at 40 Hz with a constant amplitude of $\Delta\alpha \approx \pm 0.5$ deg. Direction of the hysteresis loops with time is indicated by arrows. In this case, are all counterclockwise. The loops are also elliptical as is indicative of flow fields that are predominantly linear.
Hysteresis loops for the recalculated data sets are also plotted to demonstrate how well the unsteady model reproduces the measured characteristics. Since the flows are predominantly linear, it is clear that the model accurately reproduces the linear effects.

The flow characteristics shown in figure 9b were already discussed in section 4 (Fig. 7a). The comparison with recalculated loops highlights aft shock passage between α=5.0 deg and 6.5 deg. Some deviation is noted for the loop centered on α=5.5 deg, especially for increasing incidence and time. In this example, the unsteady model tends to make the loop more elliptical. On the whole, however, the match between the model and measured characteristics is excellent.

In figure 9c the flow characteristics are shown which were also discussed in section 4 (Fig. 7b). Although the model reproduces the SITES transition loops at α=7.0 deg, it has minor trouble with the aft moving shock loops at α=5.0 deg and 5.5 deg, shown in figure 9c. Comparing the measured and "NLR model" loops, it appears that the trends are described correctly.

The examples of figures 9a to 9c are typical of the linear and nonlinear effects that must be accounted for in unsteady aerodynamic models used in the prediction of transonic LCO for aircraft wings.
At all other flow conditions where the flows are predominantly linear, the hysteresis loops are elliptical and have a counterclockwise orientation.

Although the reproduction of individual pressure

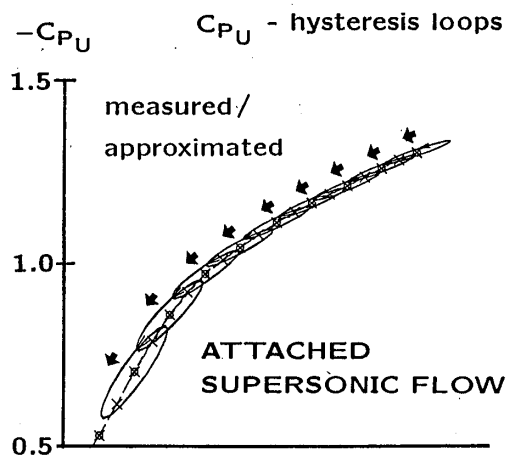

a) attached supersonic flow (WS3, pt 1)

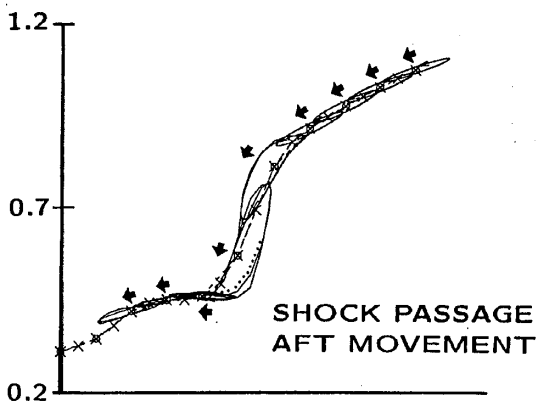

b) shock passage aft movement (WS3, pt 4)

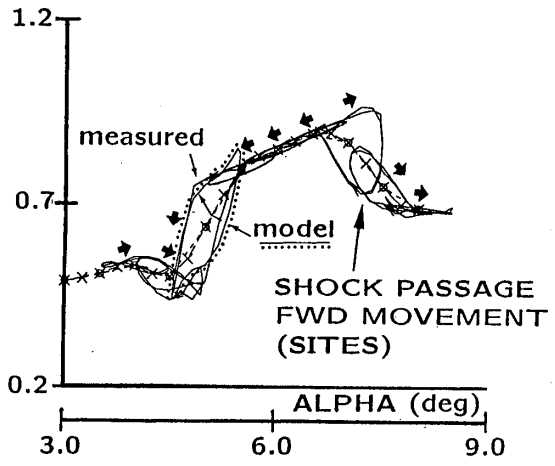

c) shock passage fwd movement (WS6, pt 7)

Fig. 9 Pressure coefficients, upper wing surface, (M=0.93), comparison of calculated hysteresis loops with experimental data.

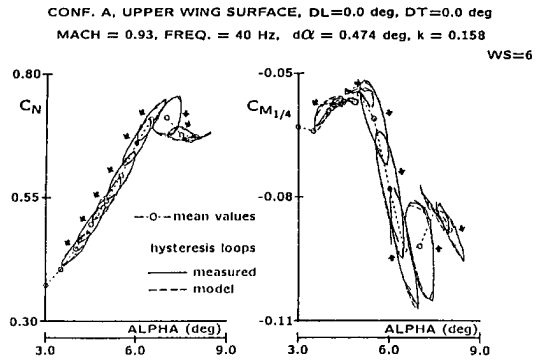

Fig. 10 Lift and moment coefficients in WS6 as function of α, (M=0.93, $\delta_{le} = 0$ deg, $\delta_{te} = 0$ deg), comparison of approximated hysteresis loops with experimental data.

variations with time is important for building the models, the chordwise integral of these variations is more important for the prediction of LCO. This is true mainly because very little chordwise bending exists in the vibration modes that are typically involved in LCO. Thus, errors in the prediction at a pressure location are generally smoothed out in the integration process.

Comparisons of measured section normal forces and pitching moments with those recalculated with the NLR model are carried out for the same conditions corresponding to figures 9a to 9c. These results are shown for the outer outboard chordwise pressure row (wing station 6) in figure 10. The same hysteresis loop format for varying mean incidence is also used in these comparisons. The measured loops are indicated by the solid lines and NLR model loops by the dashed lines.

The agreement for C_N loop predictions is excellent where as the C_m loops show slight differences between calculated and experimental values, as was expected from the individual pressure hysteresis loops. Again deviation of loop shapes from elliptic are indicative of the local nonlinearities that are embedded in the individual pressure variations. Although the C_m loops are becoming more nonlinear in these wing stations, the NLR model does quite well in following the trends. This is particularly evident in for the C_m loops above α=6.5 deg where the flows are dominated by SITES transition. Generally, the model reproduces the measured hysteresis loops of sectional coefficients very well.

Without further description of the typical flow characteristics comparisons of measured sectional

coefficients with those recalculated with the NLR model are carried out for slightly different conditions as those corresponding to figure 10.
Figures 11 and 12 show the comparisons of sectional coefficients (WS 6) for two different Mach numbers: (1) M=0.92; (2) M=0.945, respectively.
Figures 13 and 14 present the comparisons of sectional coefficients at the same wing station 6 for different flap settings: (1) lef-setting 2.5 deg; (2) lef-setting 2.5 deg , tef-setting -5.0 deg, respectively. Again the model reproduces the measured hysteresis loops of sectional coefficients very well. For the cases shown in the figures 11 to 14 it will be evident that for each case appropriate sets of modeling parameters should be determined based on their corresponding steady and unsteady aerodynamic data, because either the Mach number is changed either the configuration is changed.

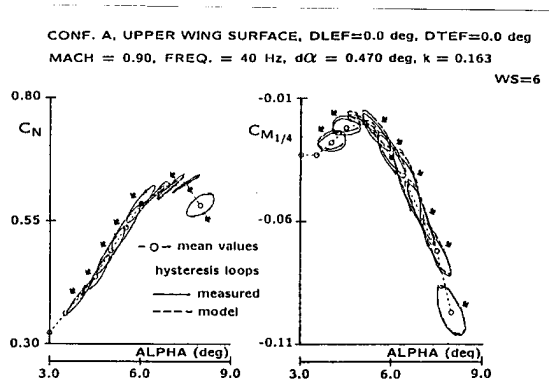

Fig. 11 Lift and moment coefficients in WS6 as function of α, (M=0.90, $\delta_{le} = 0$ deg, $\delta_{te} = 0$ deg), comparison of approximated hysteresis loops with experimental data.

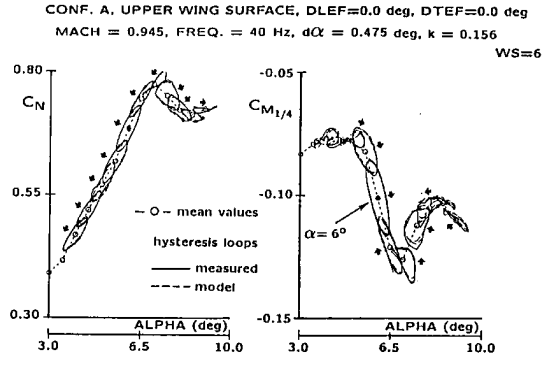

Fig. 12 Lift and moment coefficients in WS6 as function of α, (M=0.945, $\delta_{le} = 0$ deg, $\delta_{te} = 0$ deg), comparison of approximated hysteresis loops with experimental data.

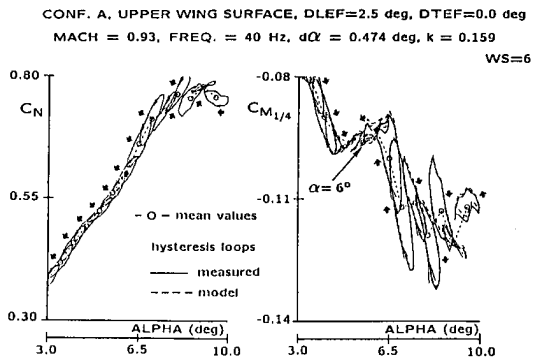

Fig. 13 Lift and moment coefficients in WS6 as function of α, (M=0.93, $\delta_{le} = 2.5$ deg, $\delta_{te} = 0$ deg), comparison of approximated hysteresis loops with experimental data.

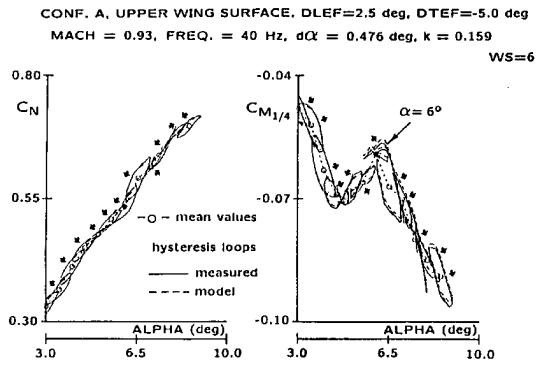

Fig. 14 Lift and moment coefficients in WS6 as function of α, (M=0.93, $\delta_{le} = 2.5$ deg, $\delta_{te} = -5$ deg), comparison of approximated hysteresis loops with experimental data.

Comparisons of sectional coefficients shown in the figures 15 and 16 were obtained by applying the identified modeling parameters for the conditions corresponding to the results of figure 13. In figure 15 the results of measured and calculated coefficients are shown for an oscillation amplitude of 0.921 deg instead of 0.474 deg.
Measured and calculated results for an oscillation amplitude of 0.254 deg instead of 0.474 deg and frequency of 56 Hz instead of 40 Hz are presented in figure 16. In these cases, the model also reproduces the measured hysteresis loops of sectional coefficients very well. For the examples shown in the figures 15 and 16 the steady data is unchanged, only unsteady data as amplitude and/or frequency are changed. This implies that the modeling parameters for the conditions corresponding to the results of figure 13 could be used.

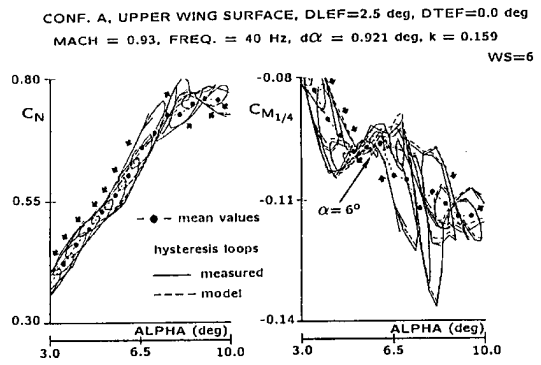

Fig. 15 Lift and moment coefficients in WS6 as function of α, (M=0.93, $\delta_{le} = 2.5$ deg, $\delta_{te} = 0$ deg), comparison of calculated hysteresis loops with experimental data.

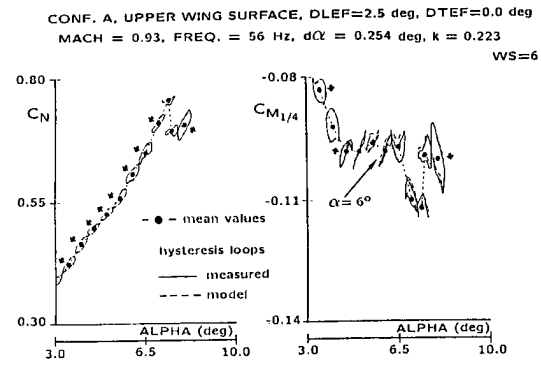

Fig. 16 Lift and moment coefficients in WS6 as function of α, (M=0.93, $\delta_{le} = 2.5$ deg, $\delta_{te} = 0$ deg), comparison of calculated hysteresis loops with experimental data.

Thus, it has been demonstrated that the NLR unsteady aerodynamic model can reproduce the highly nonlinear features of flows which are typical of transonic LCO. The next step will be to evaluate applicability of the model to the prediction of LCO as will be discussed in the following section.

7. LCO Predictions

Many LCO predictions were reported for different configurations with the LCO calculation method that contains the NLR unsteady aerodynamic model [2],[10]-[12]. Generally, steady pressure data of a full-span wind tunnel model [5] have been applied, augmented with the parameters determined in section 6, which are used in conjunction with the aerodynamic model to produce the unsteady pressures.

In particular, configuration A will be reconsidered, because this case was extensively discussed in references [2],[10]-[12]. The flight conditions for configuration A are: Mach number is 0.92, altitude is 5K ft and angle-of-attack, α_m=6.0 deg. Natural vibration modes were considered, antisymmetric and unrestrained with frequencies up to 15 Hz. The maximum number of modes then becomes 3 rigid body modes and 9 elastic modes.

Because the NLR model is based on steady and unsteady pressure data, realistic unsteady airloads could be generated only for the four outboard sections on the upper wing surface [6]. For the two remaining inboard sections on the upper surface and all six sections on the lower surface a simplified aerodynamic model was introduced. This approach still retains the important unsteady nonlinearities on outboard upper surface but permitted evaluation of the unsteady aerodynamic model in the prediction of LCO, when the simplified aerodynamic loads on surfaces different from the outboard upper wing surface are compensated by damping and stiffness forces obtained from other sources. Applying this hybrid version for the unsteady airloads in realistic LCO predictions, additional damping was taken from a linear theory flutter analysis of configuration A to account for the lag of aerodynamic damping and structural damping uncertanties.

LCO results (Fig. 17) are based on: (1) steady pressure data and modeling parameters for the conditions corresponding to the results of figure 10; (2) a variable damping which was obtained by adding g=0.02 (structural damping) to those damping values obtained for each mode from the same linear flutter analysis. The set of LCO responses shows for the indicated locations values of $\pm$5.4 g's, $\pm$3.9 g's, $\pm$0.9 g's, and $\pm$0.29 deg, respectively. As can be seen, the LCO develops uniformly and smoothly at a frequency of about 7.5 Hz (comparable with $\approx$ 68 Hz for the 1/9 scaled wind tunnel model [6]). From flight data it is estimated that LCO amplitudes for the forward accelerometer on the wing tip launcher should be of the order of 3 to 5 g's for the configuration A at the conditions used in the calculations. The predicted LCO responses, the fair comparison with experimental data and the results shown in figure 16 justify the use of the suggested aerodynamic data.

The above application of the NLR unsteady pressure model embedded in the LCO prediction method is promising; however, further analysis is continuing with the aim to extend the applicabilty of the pressure model to all known pressure ori-

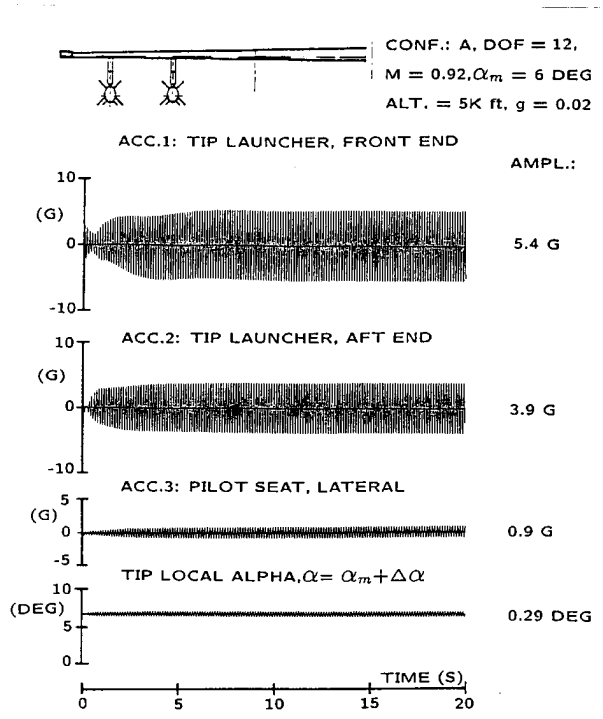

Fig. 17 Response calculation of Conf. A with state-space pressure model; 12 DOF, M = 0.92, α_m = 6 deg, alt. = 5K ft.

fice locations, angle-of-attack values and values of Mach number of the steady pressure data base [5]. Dependent on the results of that analysis the use of additional aerodynamic damping and stiffness forces from e.g. linear flutter analysis can probably be eliminated.

8. Method Improvements

The above description of the NLR pressure model shows that extensive use is made of steady and unsteady wind tunnel test data. It is clear that the effectiveness and reliability of the model strongly depends on the completeness of the experimental data base and the thoroughness of the evaluation of the model. These, however, have been obtained on a limited scale. Continued research is therefore needed to enhance the confidence in the model and to establish its applicability for wide ranges of model and flow parameters. Such research may be defined in one or more of the following directions.

1. Continued pressure and load measurements in the wind tunnel.

   The aim of this test is to extend the unsteady part of the data base, which currently corresponds to a limited number of model and flow parameter values, and so to bring it in balance with the steady part of the data base, which corresponds to an extensive set of parameter values. In particular, interest exists in collecting data for more leading-edge and trailing-edge flap deflections (because of the major impact of flap deflections on LCO responses as presented in figure 18) and denser frequency ranges (e.g. frequency sweeps). In the test use can be made of the existing wind tunnel model (Fig. 6).

2. Application of CFD.

   For model configurations and flow conditions which have not or can not be represented in a wind tunnel test program the required aerodynamic information may be obtained from Computational Fluid Dynamics techniques, steady and unsteady [13]-[15]. The current development of these techniques shows that they are very promising, even for the complicated types of flow including flow separation, but that they have not yet matured sufficiently. It is to be expected that in the near future these techniques may play a complementary role.

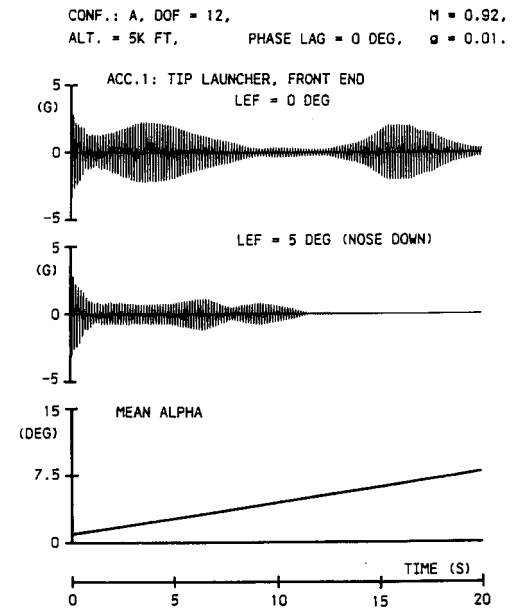

Fig. 18 Results of calculation response variations with leading edge deflections of conf. A; 12 DOF, M=0.92, α_m var., alt. = 5K ft struct. damping: g=0.01, phase lag = 0 deg

9. Conclusions

A semi-empirical method to predict LCO characteristics of fighter aircraft is being developed. The method has been described in its present form, with emphasis on the validation of an aerodynamic state-space model suggested by NLR and its capability of producing nonlinear aerodynamics which are typical of transonic LCO. Results were presented of the unsteady aerodynamic modeling and of LCO predictions. Conclusions from the investigations discussed in the current paper are summarized below.

1. It has been demonstrated that the NLR model can reproduce accurately the highly nonlinear (unsteady) features of flows which are typical of transonic LCO.

2. The NLR model is capable of producing the unsteady aerodynamic loads for a variety of conditions, suitable for use in the simulation of LCO phenomena.

3. It has been shown that the LCO prediction method with the implementation of the NLR unsteady pressure model, applying steady pressure data complemented with unsteady parameter data, and realistic structural/aerodynamic damping, is able to predict LCO responses very well in the range of conditions covered by steady wind tunnel data.

4. Continued research is needed to enhance the confidence of the model and to establish its applicability for wider ranges of model and flow parameters, including the use of advanced CFD method.

Acknowledgement

This investigation was funded by U.S. Air Force, Lockheed Martin Tactical Aircraft Systems (LMTAS), The Netherlands Ministry of Defense and National Aerospace Laboratory NLR, The Netherlands. The Netherlands Ministry of Defense with monitoring of The Netherlands Agency for Aerospace Programs (NIVR) and NLR.
The author wants to refer to the fruitful cooperation with Dr. A.M. Cunningham, Jr., LMTAS, in particular with regard to the investigation of Transonic Limit Cycle Oscillation (LCO) of fighter-type aircraft.

References

1. Cunningham, Jr., A.M., Meijer, J.J., "Semi-Empirical Unsteady Aerodynamics for for Modeling Aircraft Limit Cycle Oscillations and other Non-Linear Aeroelastic Problems", International Forum on Aeroelasticity and Structural Dynamics 1995, Manchester, UK, 26-28 June 1995.
2. Meijer, J.J., Cunningham, Jr., A.M., "Outline and Applications of A Semi-Empirical Method for Predicting Transonic Limit Cycle Oscillation Characteristics of Fighter Aircraft", International Forum on Aeroelasticity and Structural Dynamics 1995, Manchester, UK, 26-28 June 1995.
3. Meijer, J.J., "Modeling of Semi-Empirical Transonic Unsteady Aerodynamics for Predicting Limit Cycle Oscillation Characteristics of Fighter Aircraft", 20th ICAS Congress, Sorrento, Italy, September 8-13, 1996.
4. Tran, C.T., Petot, D., "Semi-Empirical Model for the Dynamic Stall of Airfoils in View of the Application to the Calculation of Responses of a Helicopter Blade in Forward Flight", Vertica, Vol.5, 1981.
5. Elbers, W.K., "Wind Tunnel Data Report 1/9-Scale F-16A Pressure Model Investigation of Shock-Induced Separation for Limit Cycle Oscillation Studies (AEDC PWT-16T Test TF-695)", General Dynamics, Fort Worth Division Report 16PR4694, September 1985, (Contract No. F33657-84-C-2034).
6. Cunningham, Jr., A.M., Boer, R.G. den, "Transonic Wind Tunnel Investigation of Limit Cycle Oscillations on Fighter Type Wings – Update", 33rd AIAA/ASME/ASCE/AHS/ASC, SDM Conference, Dallas, Texas, April 13-17, 1992.
7. Peters, D.A., "Toward a Unified Lift Model for Use on Rotor Blade Stability Analyses", 40th Annual National Forum of the American Helicopter Society, Arlington, VA, May 16-18, 1984.
8. Petot, D., Dat, R., "Unsteady Aerodynamic Loads on an Oscillating Airfoil with Unsteady Stall", 2nd Workshop on Dynamics and Aeroelasticity Stability Modeling of Rotorcraft Systems, Florida Atlantic University, Boca Raton, Florida, November 1987.
9. Dunn, P., Dugundji, J., "Nonlinear Stall Flutter and Divergence Analysis of Cantilevered Graphite/Epoxy Wings", 31st AIAA, ASME, ASCE, AHS, ASC, SDM Conference, Long Beach, California, April 2-4, 1990.
10. Meijer, J.J., "Applications of Aeroelastic Methods to Predict Flutter Characteristics of Fighter Aircraft in the Transonic Speed Range", 35th Israel Annual Conference on Aerospace Sciences, Tel Aviv/Haifa, Israel, February 15-16, 1995.
11. Meijer, J.J., Cunningham, Jr., A.M., "A Semi-Empirical Unsteady Nonlinear Aerodynamic Model to Predict Transonic LCO Characteristics of Fighter Aircraft", 36th AIAA, ASME, ASCE, AHS, ASC, SDM Conference, New Orleans, LA, April 10-12, 1995.
12. Meijer, J.J., Cunningham, Jr., A.M., "Parametric Identification of Transonic Unsteady Flow Characteristics for Predicting Flutter of Fighter Aircraft with External Stores", AGARD FDP Symposium on Aerodynamics of Store Integration and Separation, Ankara, Turkey, 24-27 April 1995.
13. Eussen, B.J.G., Hounjet, M.H.L., Zwaan, R.J., "Experiences in Aeroelastic Simulation Practices", Euromech-colloquium 349: Simulation of fluid-structure interaction in aeronautics, Göttingen, Germany, September 16-18, 1996.
14. Prananta, B.B., Hounjet, M.H.L., "Aeroelastic Simulation with Advanced CFD Methods in 2-D and 3-D Transonic Flow", Symposium Unsteady Aerodynamics 1996, RAeS, London, UK, July 17-18, 1996.
15. Prananta, B.B., Hounjet, M.H.L., "Large Time Step Aero-Structural Coupling Procedures for Aeroelastic Simulation", International Forum on Aerelasticity and Structural Dynamics, Rome, I, 17-20 June 1997.